Nuclear Instruments and Methods in Physics Research B 355 (2015) 241–245

Contents lists available at ScienceDirect

Nuclear Instruments and Methods in Physics Research B

journal homepage: www.elsevier.com/locate/nimb

Laser–plasma acceleration of electrons for radiobiology and radiation sources

L.A. Gizzi [a,b,*], L. Labate [a,b], F. Baffigi [a], F. Brandi [a,c], G.C. Bussolino [a], L. Fulgentini [a], P. Koester [a], D. Palla [a,b,e], F. Rossi [d]

[a] Intense Laser Irradiation Laboratory, INO-CNR, Via Moruzzi, 1, 56124 Pisa, Italy
[b] INFN, Sez. Pisa, Largo B. Pontecorvo, 3, 56127 Pisa, Italy
[c] Istituto Italiano di Tecnologia, Nanophysics Department, via Morego 30, 16163 Genova, Italy
[d] Universitá di Bologna e Sez. INFN, Bologna, Italy
[e] Dipartimento di Fisica, Università di Pisa, Italy

ARTICLE INFO

Article history:
Received 6 January 2015
Received in revised form 11 March 2015
Accepted 12 March 2015
Available online 16 April 2015

Keywords:
Ultra-intense laser
Laser–plasma acceleration
Radiobiology

ABSTRACT

Laser-driven acceleration in mm-sized plasmas using multi-TW laser systems is now established for the generation of high energy electron bunches. Depending on the acceleration regime, electrons can be used directly for radiobiology applications or for secondary radiation sources. Scattering of these electrons with intense laser pulses is also being considered for the generation of X-rays or γ-rays and for the investigation of fundamental electrodynamic processes. We report on laser-plasma acceleration in the 10 TW regime in two different experimental configurations aimed at generating either high charge bunches with properties suitable for radiobiology studies or high collimation bunches for secondary radiation sources with high quality and good shot-to-shot stability. We discuss the basic mechanisms and describe the latest experimental results on injection threshold and bunch properties.

1. Introduction

Laser-plasma acceleration (LPA) [1–3] driven by ultraintense Chirped Pulse Amplification (CPA) lasers [4] is being considered for the development of novel radiation sources and applications to medical sciences. In this context, given the ever increasing level of control and reliability of these schemes, compact, laser-driven accelerators may have soon an impact on radiotherapy and diagnostics in areas where electron beams with energy up to several tens of MeV are used as primary radiation. In this energy range, table-top laser systems of peak power below 10 TW can be used to drive electron acceleration and the potential for future use in a clinical environment is high [5]. A laser-driven electron accelerator may have several advantages compared to conventional linacs. First of all, given the small size of the acceleration region, the active part of the source could be enclosed in a volume, the "head" of the accelerator, as small as a few tens of cm, reducing the impact of radiation protection measures. In addition, given the possibility of transporting the laser pulse more easily than an electron beam, in the case of a medical use a single ultrashort laser system could be used to drive multiple heads for different treatment areas. In addition, higher energy bunches could be available for applications in which higher energy spread can be accepted. Finally, laser-plasma acceleration does not require UHV or high power supplies close to the utilisation area.

Moreover, given the ultra-short duration of laser accelerated bunches compared to conventional RF linacs, a new regime of ultrafast radiation biology may be activated which represents a newly emerging interdisciplinary field driven by the emerging of laser-driven particle accelerators [6]. One of the key aspects to be investigated is the very short bunch length, typical of LPA electron bunches, that leads to ultra-high instantaneous dose-rate, orders of magnitude higher than conventional sources. In view of this, preclinical studies are needed to address the radiobiological effectiveness of laser-driven electron sources compared to conventional linacs used in medical applications, with a particular attention to the intra-operatory radiation therapy (IORT) [7,8].

Along with radiobiology studies, all-optical X-ray and γ-ray sources [9] based upon Thomson or inverse-Compton scattering, are also rapidly emerging [10–14] as potentially competitive with existing similar sources based on conventional linear accelerators and already feasible with existing established acceleration regimes. Thomson scattering from free electrons is a pure electrodynamic process in which each particle radiates while

* Corresponding author at: Intense Laser Irradiation Laboratory, INO-CNR, Via Moruzzi, 1, 56124 Pisa, Italy.
E-mail address: la.gizzi@ino.it (L.A. Gizzi).

http://dx.doi.org/10.1016/j.nimb.2015.03.050
0168-583X/

interacting with an electromagnetic wave [15,16]. From the quantum–mechanical point of view Thomson scattering is a limiting case of the process of emission of a photon by an electron absorbing one or more photons from an external field, in which the energy of the scattered radiation is negligible with respect to the electron's energy. If the particle absorbs only one photon by the field (the linear or non relativistic quivering regime), Thomson scattering is the limit of Compton scattering in which the wavelength of the scattered photon observed in the particle's rest frame is much larger than the Compton wavelength of the electron. An all-optical Thomson scattering scheme can be based upon a counter-propagating configuration of two ultraintense laser pulses focused in a gaseous target. In this configuration, one of the laser pulses generates a bunch of energetic electrons while the other, counter-propagating pulse interacts with the energetic electrons generating γ-ray radiation along the bunch propagation direction.

Motivated by these considerations, we have identified LPA accelerating regimes suitable for either dosimetric and radiobiological studies or Thomson scattering aimed at validating the source for future studies [9]. Here we briefly describe the physical properties of the source, including the interaction scheme, the acceleration regimes and the characterisation of the accelerated electrons. In the first paragraph we describe the interaction scheme and list the main experimental parameters. In the second paragraph we show the main results concerning the characterisation of the laser-plasma interaction. In the third paragraph we provide an overview of basic properties of accelerated electron bunches for radiobiology studies, while in the fourth paragraph we summarise the main features of electron acceleration for Thomson scattering.

2. The experimental set up

The experiment was carried out at the Intense Laser Irradiation Laboratory (ILIL) of the INO of the CNR in Pisa using the 10 TW Ti:Sa laser system. The laser delivers 40 fs pulses up to 400 mJ on target, and features an M^2 quality factor close to 1.5 and a nanosecond contrast better than 10^9 which enables pre-plasma free interaction [17]. A summary of the laser and gas-jet target set up used for the two experimental configurations is summarised in Table 1 where $a_0 = eE_L/m_e\omega_L c = 0.85\lambda_{L,\mu m}\sqrt{I_{L,18}}$ is the laser normalised vector potential, P_0 is the laser power and $P_{cr} = 17\omega_L^2/\omega_p^2[\mathrm{GW}] = 17n_c/n_e[\mathrm{GW}]$ is the critical power for relativistic self-focusing. Here E_L, $\lambda_{L,\mu m}$, $I_{L,18}$ and ω_L are the electric field amplitude, the intensity expressed in units of 10^{18} W/cm^2, the wavelength expressed in μm and the angular frequency associated with the laser pulse, e and m_e are the electron charge and mass and n_e and $n_c = m_e\omega_L^2/4\pi e^2 = 1.1\times10^{21}/\lambda_{L,\mu m}^2[\mathrm{cm}^{-3}]$ are the plasma electron density and the critical density. In the first case "A", the laser was focused using an f/4.5 Off-Axis parabolic mirror (OAP) in a spot size of 6.2 μm FWHM, giving an intensity on target of about 2×10^{19} W/cm^2. This configuration features a relatively large divergence electron beam and is tuned for radiobiology studies where the electron beam is delivered on a sample for dosimetry and in vitro sample exposure. A different acceleration set up for extended acceleration length. Case "B" of Table 1 was based on a f/10 OAP, generating a spot size of 20 μm FWHM, giving an intensity on target of about 2×10^{18} W/cm^2. This configuration is characterised by a very low divergence electron bunch.

Table 1
Main parameters of the laser focusing configurations and the corresponding values of the gas-jet used for the two experimental configurations described here. The maximum gas-jet atom density is given, along with corresponding value of the electron density for ionisation degree N^{5+}. The last column reports the corresponding value of P_0/P_{cr}.

Case	f/#	I_L (W/cm^2)	a_0	P (bar)	N/cm^{-3}	$n_{e,5}$/cm^{-3}	P_0/P_{cr}
A	4.5	8×10^{18}	1.92	40	1.6E19	8.0E19	27
B	10	2×10^{18}	0.96	3.5	1.4E18	7.0E18	2.36

A schematic layout of the set-up inside the interaction chamber is provided in Fig. 1. In both cases the target consisted of a supersonic nitrogen (N_2) gas-jet from a rectangular nozzle with a size of 4×1.2 mm^2, with the laser propagating across the 1.2 mm side. An accurate off-line characterisation of the gas-jet profile and temporal evolution was carried out using a dedicated interferometric set up. The characterisation enabled us to obtain a back-pressure dependence of the maximum atom density for relatively high pressures above 10 bars, for which sufficient phase shift can be detected. The plot of Fig. 2 shows the temporal dependence of the maximum atom density at two back pressures of 10 and 30 bars of N_2, respectively equal to 4×10^{18} and 1.2×10^{19} atoms/cm^3. A linear behaviour of the gas-jet density vs. gas pressure is found, with a coefficient equal to 4×10^{17} for each bar of backing pressure.

An auxiliary, frequency doubled probe pulse, was used for optical shadowgraphy of the plasma along the axis perpendicular to the main laser pulse propagation direction. In addition, a Thomson imaging diagnostic system (not shown in the figure) was used to follow propagation of the main laser pulse in the plasma. Electron acceleration was characterised using a LANEX scintillator screen imaged out by a commercial reflex (Pentax100D) camera and NaI(Tl) scintillators coupled to photomultipliers. The electron spectrum was measured using a magnetic dipole equipped with permanent magnets generating a quasi-uniform magnetic field. Depending on the electron energy range, two different size dipoles were used, a 25 mm × 50 mm for high energy and a 12.5 mm × 25 mm for low energy electrons. The configuration of the low energy spectrometer allowed electron energy above 4 MeV to be detected. A tube was inserted into the chamber flange along the electron propagation direction, ending with a vacuum-air interface for the electron beam made up of a 50 μm kapton layer. The electron beam production and total charge was measured on each shot using an Integrating Current Transformer (ICT) device.

3. Laser–plasma interaction

Laser–plasma interaction plays a fundamental role in the control of the acceleration process. We used Thomson scattering from free plasma electrons and optical shadowgraphy to monitor the interaction. In the classical picture of Thomson scattering, free electrons oscillate in the laser field and, in turn, emit radiation. The properties of this scattered radiation are thus related to the properties of the medium. The particle will move mainly along the direction of the oscillating electric field, resulting in dipole electromagnetic radiation. The scattering can be described in terms of the emission coefficient defined as ϵ where $\epsilon dt dV d\Omega d\lambda$ is the energy scattered by a volume element dV in time dt into solid angle $d\Omega$ between wavelengths λ and $\lambda + d\lambda$. In our case, with the diagnostic placed perpendicularly to the plane in which the laser field oscillates, assuming a non-relativistic approximation, the emission coefficient can be written:

$$\epsilon = \frac{\pi\sigma}{2} I n_e \tag{1}$$

where σ is the Thomson differential cross section, n_e is the electron density, and I is the incident flux.

This result simply shows that the Thomson scattering provides combined information on the laser intensity and electron density. Since, in our case, knowledge on the plasma density can be derived

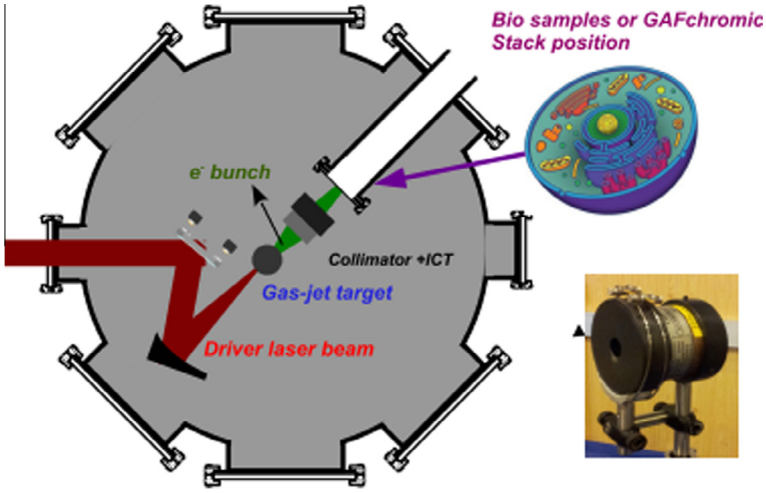

Fig. 1. Schematic layout of the experimental set-up showing the interaction configuration, the electron beam geometry and the beam extraction device.

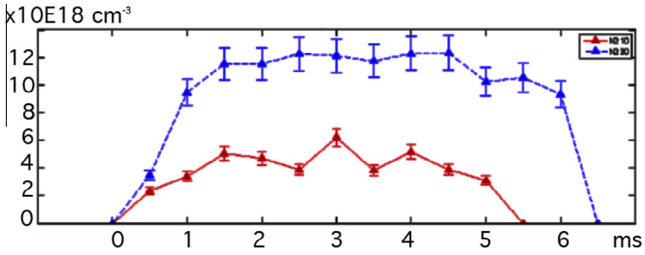

Fig. 2. Temporal evolution of the maximum gas-jet atom density for Nitrogen at two different pressures of 10 and 30 bars. The plot shows that 1 ms after the aperture of the valve the density reaches a steady-state value and remains approximately constant for about 4 ms. The peak value of the atom density scales as 4×10^{17} atoms/cm^3 per bar of pressure.

independently from the plasma interferometry, we can use Thomson scattering to derive information on the laser intensity [18]. In our experimental set up an f/3 achromatic objective combined with a colour CCD camera was used to produce a magnified image of the interaction region. The images of Fig. 3 shows the Thomson scattering emission produced along the entire laser propagation axis for the two cases of f/4.5 and f/10 focusing of the main laser pulse. The left image corresponds to the case of the f/4.5 OAP with a Nitrogen target at a back pressure of 40 bars. The image shows a ~300 μm long channel-like structure. We observe that the length of the channel is approximately twice the expected depth of focus (Rayleigh length) of 150 μm. The right image of

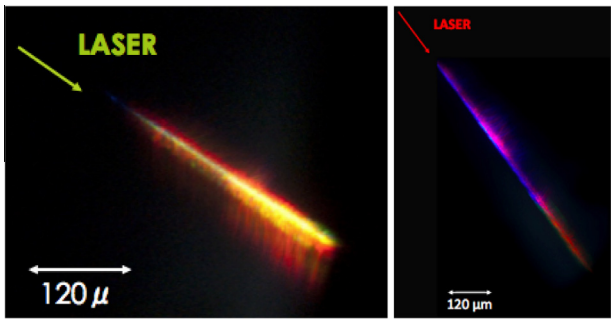

Fig. 3. Left: Thomson scattering image of the f/4.5 focusing optics showing the main features of the interaction. The waist of the laser beam is placed on the edge of the gas-jet where Thomson scattering radiation is clearly visible. Right: same image obtained with the f/10 focusing optics.

Fig. 3 shows the corresponding image obtained with the f/10 OAP at a back pressure of approximately 4 bars. In this case the length of the channel is ~600 μm, namely twice the length of the f/4.5 case. This comparison clearly shows the effectiveness of the focal length in increasing the propagation length of the laser in the plasma. Indeed these two conditions correspond to two different acceleration conditions leading to remarkably different electron bunch properties.

4. Radiobiology tailored acceleration regime

The acceleration regime with the f/4.5 OAP was optimised with the primary aim of obtaining a uniform irradiation of a large, ≈5 cm diameter area, suitable for radiobiological studies of in vitro samples. The electron energy was tuned to match the spectral features of IORT linacs, with a broad spectrum and maximum energy up to approximately 15 MeV. Back pressure of the gas-jet was scanned from 1 to 50 bars and optimum condition was found at a pressure of 40 bars, corresponding to a peak atom density just exceeding 1.6×10^{19} atoms/cm^3. In these conditions, the accelerated electrons are emitted in a cone of 0.5 rad with a relatively smooth angular distribution. The image of Fig. 4 (left) shows the lanex image at the point of sample exposure. The image clearly shows the relatively uniform electron emission over the entire exposure region with a residual, filamentary-like pattern. In order to ensure the highest uniformity, integration over a number of consecutive shots was typically used to provide a very uniform pattern, with an acceptable level of local irradiation non-uniformity [19].

The image of Fig. 4 (right) shows the corresponding raw energy spectrum of the electrons ranging from the minimum allowed by the electron spectrometer, up to a maximum exceeding 20 MeV. According to these data, both the beam pattern and the energy spectrum are well suited for radiobiological, pre-clinical validation. In fact, a careful dosimetric characterisation was carried out to obtain the dose distribution and the dose/shot on the sample by comparing experimental measurements performed using suitable stacks of GAFchromic films and solid water with GEANT4 MonteCarlo simulations of the electron beam transport interactions. The analysis shows a transverse profile of the dose distribution with a variation of the order of 10% across a 20 mm size spatial region [19]. In addition, the retrieved dose was found to be 180 mGy/shot in vacuum after 2 mm of water-equivalent layer and 60 mGy/shot in air, at the sample position, after

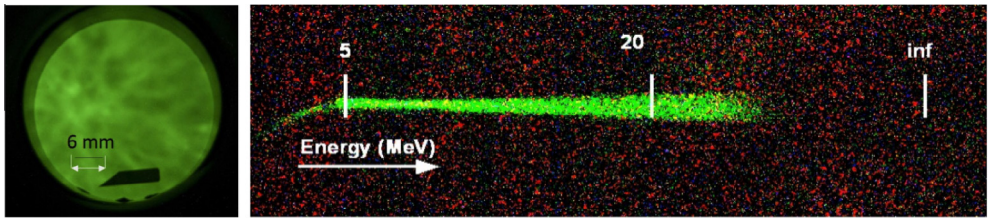

Fig. 4. Left: Lanex image of the electron bunch at the sample exposure distance from the source. Right: corresponding electron spectrum after selection and collimation of the central region.

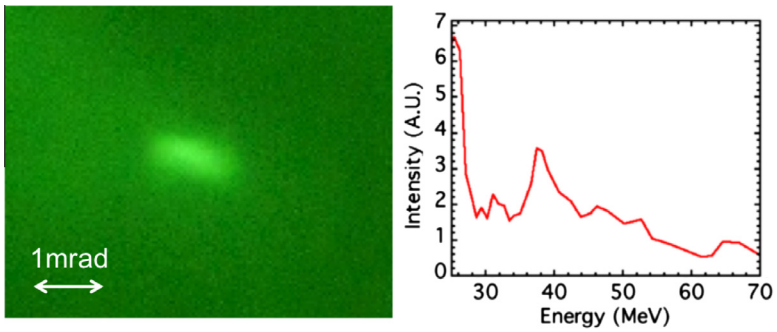

Fig. 5. left: Lanex image of the electron bunch from interaction with the f/10 OAP on Nitrogen gas-jet at 4 bar backing pressure and maximum density of 7×10^{18} cm^{-3}. Right: Corresponding energy spectrum showing a monoenergetic component at approximately 38 MeV. The laser intensity was 2×10^{18} W/cm^2.

2.2 mm thick water equivalent layer. Cumulated doses were found to be up to 10 Gy in approximately 1 min of exposure running the source at 1 Hz repetition rate. Dosimetric measurements and comparison with GEANT4 simulations also show that a strong low-energy (MeV) component, below the detection range of our electron spectrometer exists. This leads to an overall average energy of 1.5 MeV, with a total charge of 2.6 nC per shot. As summarised in the first row of Table 1, the available laser power is well above the threshold for self injection at the given plasma density, with $P_0/P_{cr} = 27$. In fact, according to [20], the power threshold for self-injection is given by $P_0/P_{cr} \geqslant 2.5$, namely a factor of eight less than the critical power of our experiment, thus ensuring very stable injection, with little fluctuations from shot to shot. The relatively high plasma density also contributes to the high injected charge observed, with the possibility of multi-bunch acceleration as observed in [21]. On the other hand, the relatively high density reduces the effective acceleration length to a fraction of the total available plasma length due to the small dephasing length $L_D \approx \lambda_p^3/\lambda_L^2$, where $\lambda_p = 3.3 \times 10^{10}/n_{e,cm^{-3}}^{1/2}[\mu m]$. In fact, in case "A", the dephasing lengths is estimated to be less than 100 μm, i.e. shorter than the observed acceleration length of 300 μm as measured from Fig. 3. This mismatch limits the maximum electron energy [22] and the short acceleration length affects the downstream angular divergence [23,24] of the electron beam due to the negligible action of transverse focusing fields.

5. Acceleration regime for Thomson scattering

A prerequisite for the set up of a Thomson scattering source is the availability of an electron source with reproducible operation, with collimated bunches, good stability and small energy spread. While these conditions are well established for conventional linac sources, laser-plasma sources require a significant optimisation before acceptable conditions are satisfied. An extensive study was carried out to optimise the acceleration regime with the f/10 OAP to obtain stable production of collimated electron bunches.

As discussed above, the propagation length in this case was 600 μm, namely approximately half of the entire gas length of 1200 μm. Compared to the previous configuration, the longer propagation length makes it possible to extend the acceleration length, increasing the angular collimation of the bunch and improving the pointing stability. A pressure scan was carried out changing the pressure from 1 to 4 bars and the injection threshold was found to occur just above 3 bars, corresponding respectively to an ion density of 1.2×10^{18} cm^{-3}.

According to numerical simulations, the ionisation degree on axis is expected to exceed N^{5+}, up to H-like N. The ionisation map of Fig. 6 was obtained for the parameters of case "A" of Table 1 via a fully consistent PIC simulation run with the code jasmine [25], in which the ionisation process was modelled using the ADK model as in [26]. The simulation shows that early during propagation in the plasma, the laser pulse self-focuses and the normalised peak potential reaches $a_0 > 2$, allowing the ionisation beyond the N^{5+} state within a radius of 3 μm from the propagation axis.

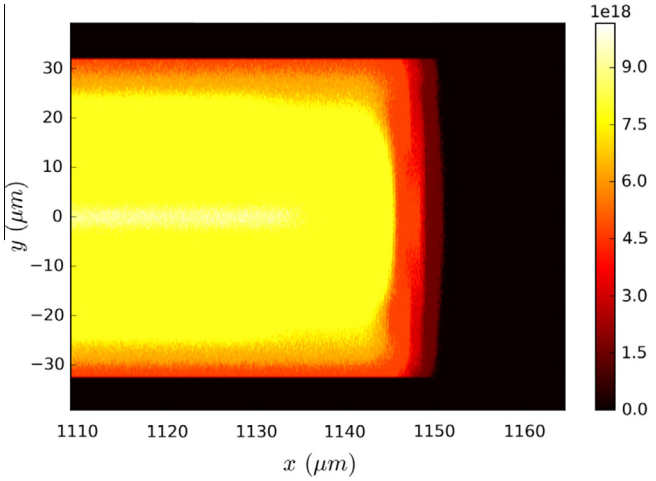

Fig. 6. Calculation of the ionisation degree of the Nitrogen gas obtained via a fully consistent PIC simulation run with the code jasmine [25].

In the experiment, the most stable operation was found between 3.5 bars and 4 bars, corresponding to an electron density of 7×10^{18} cm^{-3} and 8×10^{18} cm^{-3}. In this configuration, effective acceleration with collimated electron bunches was found, with a bunch divergence of approximately 1mrad as shown in the image of Fig. 5 (left). Spectra of electron bunches taken in this configuration showed an energy up to 60 MeV, with a monoenergetic component of less than 10% BW as shown in Fig. 5 (right). Pointing stability was found to be of the order of approximately 40 mrad. In contrast with the case "A" discussed above where the dephasing length was less than 100 μm, the dephasing length for case "B" is estimated to be approximately 3 mm, which is longer than the accelerating length of 600 μm shown in Fig. 3. In this case the acceleration is likely to be limited by diffraction or by depletion of the laser pulse, and electrons experience longitudinal accelerating and transverse focusing fields over the entire laser propagation length, approximately six time longer than in the case "A". In spite of the smaller accelerating field set by the lower electron density, case "B" leads to a higher energy and higher collimation of the electron bunch. Concerning the injection threshold, we note that as shown in the second row of Table 1, the available power P_0 in this configuration is 2.36 times the critical power P_{cr}. According to [20], for relatively high densities, close to 10^{19} cm^{-3}, the threshold for self-injection is expected to be at approximately $P_0/P_{cr} \geqslant 2.5$, a value very close to the one found in our experiment. We point out here that according to the model [20], injection is expected to occur for laser field strength $a_0 \geqslant 3$, corresponding to a laser intensity almost 10 times higher than our experimental value. At this stage we can anticipate that the observed discrepancy could partially be explained by taking into account the actual evolution of the laser pulse during the propagation in the plasma. In fact, as discussed above, a strong self-focusing is predicted by numerical simulations and laser intensity is expected to increase significantly. In addition, other important processes like guiding, diffraction, self-steepening and depletion, a self-consistent description of this regime is necessary to correctly evaluate the self-injection process in our experimental conditions. A systematic numerical study of our acceleration regime is currently in progress to examine these issue.

6. Conclusions

We identified two different experimental configurations of laser-plasma acceleration based on a 10 TW laser pulse focused respectively with an f/4.5 OAP and an f/10 OAP on a 1.2 mm long Nitrogen gas-jet and tailored for two different applications. In the first configuration, an electron bunch with a broad energy spectrum extending above 20 MeV and large angular divergence was characterised in view of radiobiology experiments using large in vitro samples. In this case a high density gas-jet and a high laser intensity, with $a_0 = 1.92$ were used to ensure stable injection and reproducible operation at high bunch charge of 2.6 nC. In the second configuration a high spectral quality self-injection regime was identified at an electron density just above the injection threshold to drive a Thomson scattering X-ray source. In this case longer focal length OAP was used to ensure extended propagation in the gas-jet. Self-injection threshold was found to occur at an electron density of 7×10^{19} cm^{-3}, at a value of $P_0/P_{cr} \geqslant 2.36$, a value very close to the one expected from self-injection models. Both acceleration conditions were found to be highly reproducible and are currently established as laser driven electron sources for important applications to radiobiology and secondary sources.

Acknowledgements

We acknowledge financial support from the CNR funded Italian research Network ELI-Italy (Attoseconds) and from the Italian Ministry of Health through the project GR-2009-1608935 (d.i. Agenas). We also acknowledge contribution from the MIUR-FIRB project SPARX (Sorgente Pulsata Auto-Amplificata di Radiazione X) and from the INFN funded (CN5) project γ-ray Emitter from Self-Injected Thomson Scattering (γ-RESIST). The work at ILIL was carried out in the framework of the CNR High Field Photonics Unit (MD.P03.034). We acknowledge the CINECA Grant N. HP10CZX6QK2012 for the availability of high performance computing resources and the INFN APE project for the availability of the QUonG cluster.

References

[1] J. Faure et al., Lett. Nat. 431 (2004) 541.
[2] W.P. Leemans et al., Nat. Phys. 2 (2006) 696.
[3] D. Giulietti et al., Phys. Plasmas 9 (2002) 3655 (letter).
[4] D. Stickland, G. Mourou, Opt. Commun. 56 (1985) 219.
[5] L. Labate et al., in: E. Esarey, C.B. Schroeder, W.P. Leemans, K.W.D. Ledingham, D.A. Jaroszynski (Eds.), Laser Accel. Electrons, Protons, Ions II; Med. Appl. Laser-Generated Beams Part. II; Harnessing Relativ. Plasma Waves III, Proceedings of SPIE, vol. 8779, SPIE, 2013.
[6] V. Malka, J. Faure, Y. Gaudel, Mutat. Res. 704 (2010) 142.
[7] S. Righi, E. Karaj, G. Felici, F.D. Martino, J. Appl. Clin. Med. Phys. 14 (2013).
[8] A. Gamucci et al., AIP Conf. Proc. vol. 1209, 2010, pp. 39–42.
[9] L.A. Gizzi et al., Nucl. Instr. Meth. Phys. Res. Sect. B Beam Interact. Mater. Atoms 309 (2013) 202.
[10] G. Sarri et al., Phys. Rev. Lett. 113 (2014) 224801.
[11] S. Chen et al., 2013, vol. 155003, p. 1.
[12] N.D. Powers et al., Nat. Photonics 8 (2013) 28.
[13] K.T. Phuoc et al., Nat. Photonics 6 (2012) 308.
[14] L. Gizzi et al., Eur. Phys. J. Spec. Top. 175 (2009) 3.
[15] P. Tomassini, a. Giulietti, D. Giulietti, L.a. Gizzi, Appl. Phys. B 80 (2005) 419.
[16] P. Tomassini et al., IEEE Trans. Plasma Sci. 36 (2008) 1782.
[17] A. Giulietti et al., Phys. Plasmas 13 (2006) 093103.
[18] L.A. Gizzi et al., IEEE Trans. Plasma Sci. 39 (2011) 2954.
[19] D. Lamia, Nucl. Instr. Meth. Phys. Res. A 786 (2015) 113.
[20] C. Benedetti et al., Phys. Plasmas 20 (2013) 103108.
[21] A. Giulietti et al., Phys. Rev. Lett. 101 (2008) 105002.
[22] E. Esarey, C. Schroeder, W. Leemans, Rev. Mod. Phys. 81 (2009) 1229.
[23] C.M.S. Sears et al., Phys. Rev. Spec. Top. – Accelerators and Beams 092803 (2010) 1.
[24] R. Lehe et al., Phys. Rev. Spec. Top. – Accelerators and Beams 17 (2014) 121301.
[25] F. Rossi et al., AIP Conf. Proc. 1507 (2012) 184.
[26] M. Chen et al., J. Comput. Phys. 236 (2013) 220.